International Journal on Magnetic Particle Imaging
Vol 3, No 1, Article ID 1703020, 5 Pages

Infinite Science Publishing

Research Article

MPI Flow Analysis Toolbox exploiting pulsed tracer information - an aneurysm phantom proof

Jochen Franke[a,b,†,*] · Romain Lacroix[a,†] · Heinrich Lehr[a] · Michael Heidenreich[a] · Ulrich Heinen[c] · Volkmar Schulz[b]

[a] Bruker BioSpin MRI GmbH, Ettlingen, Germany
[b] Physics of Molecular Imaging Systems, University RWTH Aachen, Aachen, Germany
[c] University of Applied Sciences Pforzheim, Pforzheim, Germany
[†] These authors contributed equally to this work
[*] Corresponding author, email: jochen.franke@bruker.com

Received 11 November 2016; Accepted 2 March 2017; Published online 23 March 2017

Abstract

Assessment of flow parameters provides insight into (patho-)physiology and thus is a common tool in the field of cardiology to screen for or to evaluate and stage cardiovascular diseases. In this work, we present a Flow Analysis Toolbox for Magnetic Particle Imaging datasets highlighting pulsed tracer information. The presented tool uses time as well as frequency signal processing approaches and exploits an Optical Flow analysis to extract quantitative 4D velocity vector fields. In this work, we successfully estimate flow patterns in a nonrealistic aneurysm shaped vessel phantom exploiting pulsed tracer information by means of an easy-to-use Flow Analysis Toolbox.

I. Introduction

Flow estimation is a common tool in the field of cardiology to screen for or to evaluate and stage cardiovascular diseases. Here, Ultrasound (US) based approaches making use of the Doppler-effect [1] are the most common used methods in cardiology. More complex flow estimations can be derived from X-Ray DSA (Digital Subtraction Angiography) by extracting the time and space derivative of the contrast product [2], or Magnetic Resonance Imaging (MRI) datasets exploiting phase information [3] of moving structures. US-based approaches are fast and cheap but with limited 3D capabilities, DSA suffers from the pitfalls of projective geometry while using ionizing radiations, and MRI-based approaches permit for 4D flow estimations with high spatial resolution on the expense of long acquisition times. By making use of the intrinsic fast 3D repetition rates, Magnetic Particle Imaging (MPI) [4] by its extremely short acquisition times enables estimation of 4D velocity vector fields by analyzing pulsed tracer information by optical flow techniques firstly introduced by R. Lacroix [5, 6]. A recent publication [7] suggests MPI being a useful candidate to evaluate hemodynamics in aneurysms with high temporal resolution and without the need for ionizing radiation as used in the gold standard DSA. In this work, a phantom prove of a Flow Analysis Toolbox is presented.

II. Methods

II.I. 4D Flow Analysis Toolbox using an Optical Flow algorithm

To allow the extraction of (blood) flow estimates from 4D MPI image data highlighting pulsed tracer information,

a Flow Analysis Toolbox (Bruker BioSpin MRI GmbH, Germany) was generated based on previous work [6].

This toolbox, implemented in MATLAB® (The MathWorks, Inc., USA), uses time as well as frequency signal processing approaches to extract from reconstructed MPI datasets the velocity information from time-intensity-curves (TIC). In this approach only signal components within narrow bands around the tracer pulse frequency (i.e. for in vivo studies the heart frequency) and its harmonics up to a user defined threshold are used for analysis. Thus, only a small part of the spectrum is exploited for the flow reconstruction. This is a viable assumption already used in DSA flow estimation [2], as blood flow occurs in answer to the periodic wall contractions, and as such should be periodic, or nearly periodic. To circumvent the pitfall of spatio-temporal extrema of the TICs, i.e. where time- and space-derivative nullifies, the Hilbert transform is used to complement the processed TICs. The Hilbert transform basically creates a quadrature signal, i.e. a time-shifted signal of the original sequence that undergoes a phase shift of $\pi/2$ (see [6], section 3.2.2 and 3.2.3 for more details). With this, a representation of the signal at every point in space p within the FoV is preserved by a time dependent instantaneous phase $\rho(p,t)$ as well as an instantaneous modulation depth $M(p,t)$, called henceforward modulus. By computing the spatial gradient vectors of $\rho(p,t)$ and the displacement $v(p,t)$ using Optical Flow algorithms [8], quantitative velocity vector fields are extracted.

II.II. Phantom experiment

Tracer modulator device

The flow system (see Fig. 1) was realized by two reservoirs, placed above the Faraday cage, one with tracer fluid and the other with demineralized water. Each reservoir was connected to one tube, while the flow was controlled for each tube by a straightway diaphragm valve system, namely a Lego Mindstorm© unit. Both tubes were compressed alternately with a defined frequency by the modulator device (see Fig. 2).

Close to the actual phantom, both tubes were connected with a 3-way junction for mixing the two streams, resulting in quasi continuous flux with modulated tracer concentration. The modulated and stabilized water-tracer mixture finally was injected into the phantom and drained thereafter into a reservoir.

Aneurysm phantom

A phantom of a nonrealistic aneurysm shaped vessel (see Fig. 3) was used. The modulated water-tracer mixture flux was injected with a silicon tube (ID = 4 mm) into the irregular aneurysm structure. To generate the modulated water-tracer flux, the modulator device was set

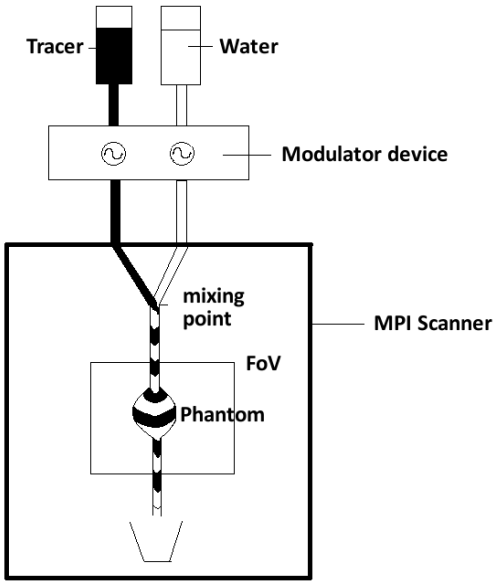

Figure 1: Schematic experimental setup, sketch adapted from [6].

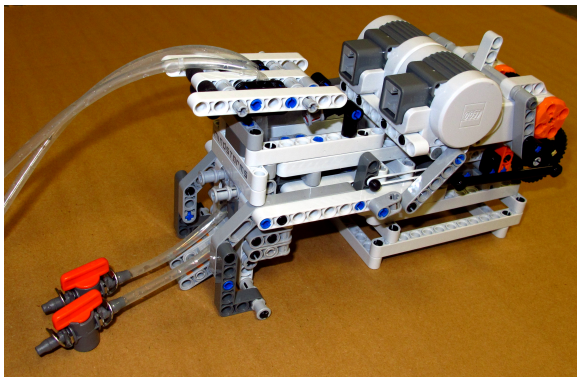

Figure 2: Photograph of the tracer modulator device, realized by a Lego Mindstorm© unit.

to a modulation frequency $f_{\mathrm{mod}} \approx 2.3$ Hz. By using this modulation protocol, the flow rate

$$Q = \frac{\Delta V}{\Delta t} \tag{1}$$

of this phantom set up was measured prior to the MPI experiment three times to facilitate the velocity estimation in the injection point.

For the MPI experiment, the tracer reservoir was filled with Resovist (Bayer Schering Pharma AG, Germany) diluted to $c \approx 24\,\mu$Mol(Fe)/ml.

MPI Data Acquisition

In the MPI mode of the MPI-MRI hybrid system characterized in [9] (Bruker BioSpin MRI GmbH, Germany) and

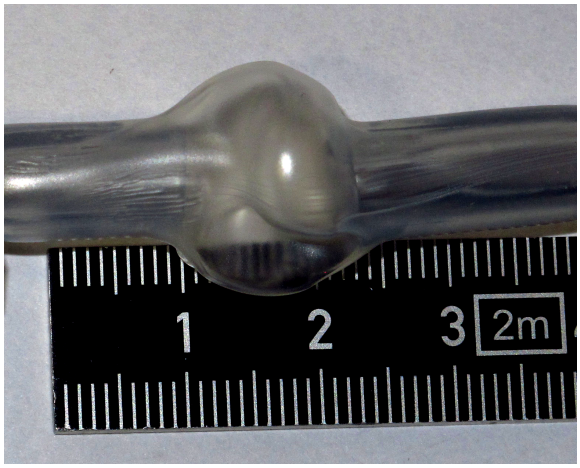

Figure 3: Photograph of the aneurysm phantom.

the usage of Drive Field amplitudes of $A_{\mathrm{DF\ X,Y,Z}} = 14\,\mathrm{mT}$ and a Selection Field gradient slope of $G_{\mathrm{SF\ max}} = 2.2\,\mathrm{T/m}$, 5000 3D datasets with a repetition time of $TR \approx 21\,\mathrm{ms}$ were acquired with an acquisition bandwidth of $BW_{\mathrm{acq}} = 625\,\mathrm{kHz}$. During MPI data acquisition, the flux of a modulated water-tracer mixture was released to flush the phantom.

MPI Image Reconstruction

For the system function based image reconstruction, the modulated water-tracer mixture bolus passage was selected manually (401 repetitions) and background corrected by using data acquired prior to the bolus passage. With a Kaczmarz algorithm [10] with 40 iterations and a relative regularization parameter of $\lambda = 0.01$ and $SNR_{\mathrm{threshold}} = 30$, max mixing order = 20 (resulting in 2000 available frequency components) of a matching and denoised [11] system matrix (matrix size $33 \times 33 \times 20$ covering a FoV = $33 \times 33 \times 20\,\mathrm{mm}^3$), the MPI raw data were reconstructed using ParaVision® (Bruker BioSpin MRI GmbH, Germany).

Flow estimation

The reconstructed time-resolved 3D MPI data were spatially interpolated to an isotropic resolution of $0.5 \times 0.5 \times 0.5\,\mathrm{mm}^3$ and cropped in Y-direction to approximately the Drive Field FoV and fed afterwards into the Flow Estimation Toolbox. An automatic Fourier analysis of Time Intensity Curves (TIC) was used to estimate the modulation frequency. This modulation frequency was selected for narrowband filtering together with the 3 following harmonics thereof. A Tikhonov regularization parameter λ was set to 10^{-18} of the magnitude of the maximum phase gradient. After determination of a time dependent instantaneous phase $\phi(p,t)$ as well as an instantaneous modulation depth $M(p,t)$ of the 3D+t MPI dataset, 3D velocity vector fields of 140 consecutive time points (marked in gray in Fig. 6) with an increment of 21.5 ms were estimated. As constraint for the velocity estimation, the limit S representing the aneurysm walls was derived by iso-surfacing of the 4D MPI dataset integrated over time (see Fig. 4).

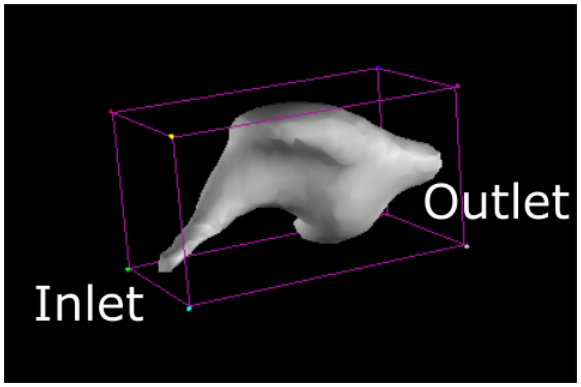

Figure 4: 3D rendering of the bolus MPI aneurysm phantom data. To delineate the aneurysm phantom volume, the 4D MPI dataset was integrated over time to eliminate the pulsed tracer pattern used for the optical flow analysis. The resulting iso-surface was used as limit S in the Flow Analysis Tool as one constraint for the velocity estimation.

Analysis of the reconstructed velocity vector fields

To assess the results of the Flow Analysis Toolbox, the reconstructed individual 140 3D velocity vector field estimates were averaged over time to 24 bins using 20 consecutive velocity vector fields, assuming the flow magnitude and direction being approximately constant within the sequences of 0.43 s duration. The averaged 4D velocity vector fields were analyzed in terms of flow directions, velocity profiles and velocity magnitudes as well as in terms of the principle of mass conservation. For this purpose, the velocity surface integral of the normal component of the XZ-planes was calculated within the limit S, and multiplied by the area spanned up by S. To define the limit S of the respective slice, the iso-surface derived from the integrated 4D MPI dataset already used as flow estimation constraint (see Fig. 4 and Fig. 5 red iso-surface) was utilized. For validation of the principle of mass conservation, the inflow (first XZ-plane) and the outflow (last XZ-plane) was compared.

III. Results

III.I. Phantom experiment

The flow rate of the experimental setup was manually determined to $\bar{Q} = 6.2\,\mathrm{ml/s}$ prior to the MPI experiments. With this, the plug-flow velocity at the aneurysm

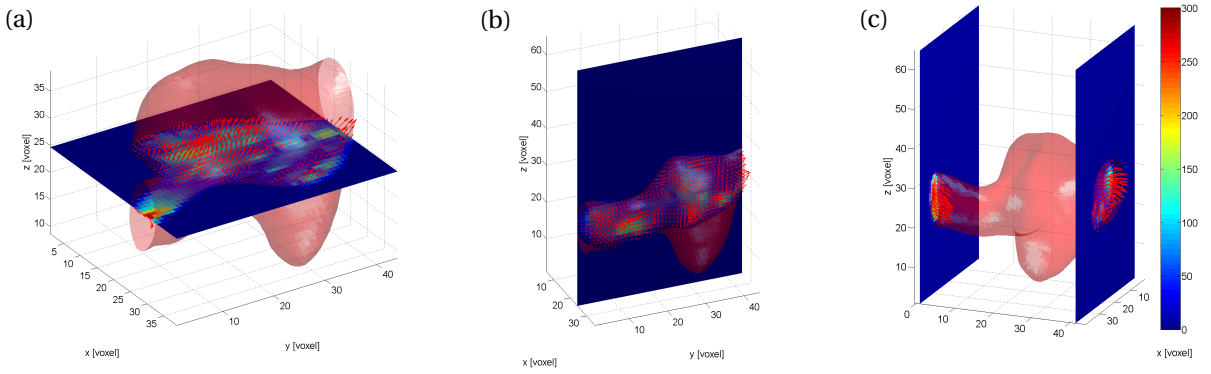

Figure 5: Result of the 4D flow estimates in different 3D views using 3D quiver representation (red arrows). The red translucent surface (the limit S) represents the aneurysm walls, while the color code of the shown planes encode $|v|$ in mm/s. In all three views, the aneurysm inlet is on the left side and the aneurysm outlet is on the right side. (a) XY-plane, (b) YZ-plane, and (c) the inlet and the outlet in two color coded XZ-planes.

inlet (ID = 4 mm) can be assessed to approximately $v_{\text{plug}} = 490$ mm/s. This translates at a temporal resolution of $\Delta t = 21$ ms into a maximum wave propagation Δx per frame

$$\Delta x = v_{\text{plug}} \cdot \Delta t = 10.3\,\text{mm}. \tag{2}$$

From the reconstructed 4D MPI images, TICs of single voxels were determined (see Fig. 6), while a Fourier analysis yielded a modulation frequency of $f_{\text{mod}} = 2.53$ Hz. From these values the spatial wavelength of the tracer modulation at the inlet can be derived to:

$$\lambda = \frac{v_{\text{plug}}}{f_{\text{mod}}} \approx 200\,\text{mm}. \tag{3}$$

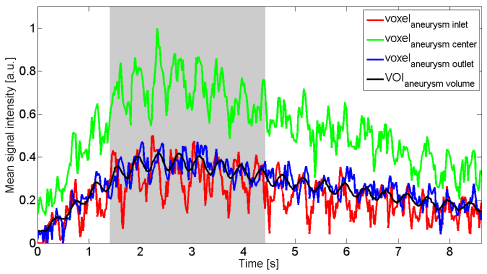

Figure 6: Time Intensity Curves (TICs) from a single voxel at the aneurysm inlet (red), center (green) and outlet (blue) as function of time, as well as the mean signal intensity of a VOI (black) corresponding to the outer surface of the aneurysm, i.e. the volume spanned up by the limit S. The gray area depicts the 140 consecutive 3D volumes, for which the 4D velocity vector field was estimated.

With this, the capture range Δx_{max}, which describes the maximum distance between two phasefronts that allows a proper registration, can be derived to:

$$\Delta x_{\text{max}} = \frac{\lambda}{2} = 100\,\text{mm}, \tag{4}$$

which is approximately 10 times larger than the maximum wave propagation Δx per frame expected in the phantom experiment. Thus, the applied tracer modulation wave can be tracked with a temporal resolution of 21.5 ms and a spatial resolution of 1 mm.

The computation time for a 4D velocity vector field estimation was approximately 13 minutes (Intel Quad-Core, 2.8 GHz).

Representative time points of the 4D velocity vector fields are plotted (see Fig. 5 and supplementary video information of the 4D velocity vector field) using a quiver representation as well as color coded planes depicting the velocity magnitude. Additionally, the expected aneurysm wall - derived from the integrated 4D MPI data - is plotted as translucent red iso-surface. The estimated velocity vector fields exhibit coherent stream line patterns with a central main flow direction from the inlet to the outlet. Two main vortices, corresponding to the two main aneurysm lobes, are visible.

The velocity vectors are aligned parallel to the boundaries and diminish towards the boundaries (see Fig. 5(a)). At the inlet as well as the outlet, the velocity profiles exhibit elliptical shapes (see Fig. 5(c)). The maximum velocity magnitude within the inlet was determined to $v_{\text{max}} = 300$ mm/s. From the velocity surface integrals, the mean flow rates were determined to $\bar{Q}_{\text{in}} = 1.28$ ml/s and $\bar{Q}_{\text{out}} = 1.32$ ml/s for the inlet and the outlet, respectively.

IV. Discussion

Using the Flow Analysis Toolbox, coherent velocity vector fields with a central main flow direction from the inlet to the outlet of the aneurysm were estimated, preserving the no-slip condition at solid interfaces in fluid mechanics. This can be seen in Fig. 5(a)–(c), where the velocity vectors are aligned parallel to the boundaries

and diminish at the boundaries. The two main vortices, corresponding to the two main aneurysm lobes, are reasonable in terms of flow direction, flow separation and flow patterns. At the inlet as well as the outlet, the velocity profiles exhibits elliptical shapes (see Fig. 5(c)) which are characteristic for laminar flows in tubes. Assessing the reconstructed velocity magnitude of the inlet ($v_{\max} = 300\,\mathrm{mm/s}$), there still is a significant difference to the expected plug-flow velocity $v_{\mathrm{plug}} = 500\,\mathrm{mm/s}$. By paying attention to the principle of mass conservation in Y-direction, there is a residual error less than 3 % comparing inlet and outlet. Larger errors were observed paying attention to the principle of mass conservation evaluating the inlet and the center of the aneurysm phantom.

While the reconstructed spatial image resolution of $1 \times 1 \times 1\,\mathrm{mm}^3$ might be a limiting factor for a precise flow magnitude quantification in small structures, significant changes in the inner diameter of the phantom causing a disturbed flow conjugated with partial volume effects in the image as well as the flow reconstruction could introduce additional errors. While averaging the reconstructed 4D velocity vector fields can be seen as valid step in phantom studies providing a quasi-continuous flow direction and magnitude paired with static wall constrains, this might not reflect the truth in much more complex flow situation. By evaluating e.g. in vivo datasets, pulsatile flows in terms of magnitude and directions as well as moving structures coexist within one heart cycle. Thus, more reasonable approaches such as gating enables reflecting complex (patho-) physiological processes.

To fully quantify the estimates of the presented Flow Analysis Toolbox, a much simpler experiment for which an analytic solution is known, such as straight tubes, has to be performed. Furthermore, by introduction of additional constraints reflecting the laws of fluid mechanics, the physical faithfulness of this Flow Analysis Toolbox could be further optimized. In future analysis it might be of interest investigate different approaches of wall estimates used as constraint for the Flow Analysis accounting for stagnating flow or dynamic boundary conditions.

Additionally, to mimic and validate pulsatile physiological flow patterns, further experiments with constant tracer administration and the usage of more sophisticated flow pump systems have to be performed. Nevertheless, despite *in vivo* scenarios, there are plenty of (technical) applications which do not require pulsatile flow patterns justifying a constant main flow with pulsed tracer information as used in this study. Besides, the described method copes with both scenarios of either constant flow over time with a modulated tracer concentration or pulsatile flow with a continuous tracer administration resulting in a modulated tracer concentration. With the presented results it was revealed that MPI in combination with optical flow analysis is an appropriate candidate for qualitative flow estimation.

To summarize, we have demonstrated 4D velocity vector field estimations in an aneurysm phantom exploiting pulsed tracer information by means of a Flow Analysis Toolbox. As input a reconstructed time-resolved 3D MPI dataset, corresponding to a total acquisition time of approx. 8.6 seconds, was used to successfully estimate quantitative and time-resolved 3D velocity vector fields.

Compared to other methods, MPI-derived 4D flow analysis allows for minimized acquisition times even without the need for breath holding cf. MRI techniques and without usage of any ionizing radiation cf. DSA techniques and furthermore without the susceptibility of angular errors known from US Doppler techniques. With this principal demonstration, a new method is introduced which may be further developed into a future-routine flow analysis approach in patient care.

References

[1] D. L. Franklin, W. Schlegel, and R. F. Rushmer. Blood flow measured by Doppler frequency shift of back-scattered ultrasound. *Science*, 134(3478):564–565, 1961.

[2] O. Bonnefous, V. M. Pereira, R. Quared, O. Brina, H. Aerts, R. Hermans, F. van Nijnatten, J. Stawiaski, and D. Ruijters. Quantification of arterial flow using digital subtraction angiography. *Med. Phys.*, 39(10):6264–6275, 2012. doi:10.1118/1.4754299.

[3] M. T. Vlaardingerbroek and J. A. Boer. *Magnetic Resonance Imaging: Theory and Practice*. Springer, Berlin/Heidelberg, 2003. doi:10.1007/978-3-662-05252-5.

[4] B. Gleich and J. Weizenecker. Tomographic imaging using the nonlinear response of magnetic particles. *Nature*, 435(7046):1214–1217, 2005. doi:10.1038/nature03808.

[5] R. Lacroix, J. Rahmer, O. M. Weber, H. G. Morales, and S. Makram-Ebeid. Flow assessment from in vitro and in silico dynamic MPI data. In *International Workshop of Magnetic Particle Imaging*, pages 64–65, 2014.

[6] R. Lacroix. *3D Optical flow analysis of a pulsed contrast agent in the bloodstream: Application to virtual angiography and Magnetic Particle Imaging*. Télécom Bretagne; Université de Bretagne Occidentale, 2015. HAL Id : tel-01298049, version 1.

[7] J. Sedlacik, A. Frölich, J. Spallek, N. D. Forkert, T. D. Faizy, F. Werner, T. Knopp, D. Krause, J. Fiehler, and J.-H. Buhk. Magnetic Particle Imaging for High Temporal Resolution Assessment of Aneurysm Hemodynamics. *PLOS ONE*, 11(8):e0160097, 2016. doi:10.1371/journal.pone.0160097.

[8] B. D. Lucas and T. Kanade. An Iterative Image Registration Technique with an Application to Stereo Vision. In *International Joint Conference on Artificial Intelligence*, pages 674–679, 1981.

[9] J. Franke, U. Heinen, H. Lehr, A. Weber, F. Jaspard, W. Ruhm, M. Heidenreich, and V. Schulz. System Characterization of a Highly Integrated Preclinical Hybrid MPI-MRI Scanner. *IEEE Trans. Med. Imag.*, 35(9):1993–2004, 2016. doi:10.1109/TMI.2016.2542041.

[10] S. Kaczmarz. Angenäherte Auflösung von Systemen linearer Gleichungen. *Bulletin of the International Academy Polonica Sciences Letters A*, 35:355 – 357, 1937.

[11] A. Weber, J. Weizenecker, U. Heinen, M. Heidenreich, and T. M. Buzug. Reconstruction Enhancement by Denoising the Magnetic Particle Imaging System Matrix Using Frequency Domain Filter. *IEEE Trans. Magn.*, 51(2):7200105, 2015. doi:10.1109/TMAG.2014.2332612.